Available online at www.sciencedirect.com
SCIENCE DIRECT®
Talanta 65 (2005) 1008–1014
Talanta
www.elsevier.com/locate/talanta

Np(IV)/Np(V) valence determinations from Np L3 edge XANES/EXAFS

Melissa A. Denecke*, Kathy Dardenne, Christian M. Marquardt

Forschungszentrum Karlsruhe GmbH, Institut für Nukleare Entsorgung, Postfach 3640, D-76021 Karlsruhe, Germany

Received 12 May 2004; received in revised form 5 August 2004; accepted 26 August 2004
Available online 1 October 2004

Abstract

X-ray absorption near edge structure (XANES) spectroscopy for in situ metal valence determination has become a powerful analytical tool in heterogeneous systems. This is in part because it is applicable without prior separation procedures. For some systems, however, determining the oxidation state from XANES spectra is not straightforward and caution must be used. We show that the analysis of L3,2 edge EXAFS (extended X-ray absorption fine structure) spectra is better suited to distinguish between Np(IV) and Np(V) than from their XANES spectra. Whereas evidence for the oxidation of Np(IV) in solution samples from their Np L3 XANES is unclear, their EXAFS data unequivocally reveals Np(V) formation in the solutions.

Keywords: Valence determination; Np; XANES; EXAFS

1. Introduction

Because it can be applied without prior separation procedures, in situ metal valence determination using X-ray absorption near edge structure (XANES) spectroscopy has become a powerful analytical tool in heterogeneous systems. Numerous examples are found in the literature, where oxidation state determinations have been successful for various metals (e.g., transition metals [1], group Vb elements [2], lanthanide [3,4], and actinide metals [5]) in different matrices, many of which are very heterogeneous. For some systems, the XANES structure and their energy position between different oxidation states are dramatically different such as the single-peak and double-peak L3 XANES structure in Ce(III) and Ce(IV) compounds, respectively [4]. Oxidation state determinations, including quantification of valence mixtures, are straightforward for these systems. Caution must be used, however, for valence determinations from XANES measurements for metals whose XANES exhibit only modest differences between their various oxidation states. An example of this is distinguishing between tetravalent and pentavalent states of neptunium from their L3,2 edge XANES spectra. One factor leading to difficulties is, due to the differences in XANES spectral resonance features between Np(IV) and Np(V), the energy position of Np(IV) appears above that for Np(V). This is in reverse order of the expected simple increase in ionization energy with increasing valence state of the absorbing atom. This point was also reported by Farges et al., for uranium [6]. Another factor, which can be crucial in the Np(IV)/Np(V) determination, involves the intensity of the most prominent XANES feature, the white line. Np(IV) L3 XANES generally exhibit intense white lines, whereas the white line in Np(V) spectra is comparably reduced. However, the white line intensity also varies with the degree of condensation of the sample phase [7,8]. These intensity differences can lead to errors in individual concentration determinations of Np(IV) and Np(V) in mixtures through linear combination of XANES spectra from reference compounds, if the degree of condensation of the unknown differ highly from the reference compounds.

The present communication illustrates the advantage of analyzing the extended X-ray absorption fine structure (EXAFS) spectra instead of XANES spectra to unambiguously differentiate between Np(IV) and Np(V), even in valence mixtures. Comparison of Np L3 edge XANES from a con-

* Corresponding author. Tel.: +49 7247 82 5536; fax: +49 7247 82 3927.
E-mail address: melissa@ine.fzk.de (M.A. Denecke).

0039-9140/$ – see front matter © 2004 Elsevier B.V. All rights reserved.
doi:10.1016/j.talanta.2004.08.034

densed system (hydrolyzed Np(IV)) with the Np^{4+} aquo species, as well as a comparison with Np(IV) and Np(V) aqueous solutions containing dissolved humic substances (HS) are provided to illustrate the difficulties encountered when analyzing XANES data for neptunium valence determinations. In order to demonstrate the advantage of identifying the presence of Np(V) in Np(IV)/Np(V) mixtures from their EXAFS, we perform a slow in situ photo-oxidation of a 1 mM aqueous solution of Np(IV) to Np(V) at $-\log[H^+]$ 1.8 while recording the Np L3 edge XANES/EXAFS.

2. Experimental

2.1. Preparation of the Np(IV) stock solution, $-log[H^+]$ ~1.8 sample and hydrolyzed Np(IV) precipitate

One milli litre of a ~36 mmol L^{-1} Np(V) solution in 1 mol L^{-1} $HClO_4$ is diluted with 2 mL 1 mol L^{-1} $HClO_4$, transferred to a electrochemical cell, and reduced to Np(III) at −0.2 V versus a Ag/AgCl reference electrode for 30 min. The Np(III) solution is then oxidized to Np(IV) at +0.3 V against the Ag/AgCl reference electrode until the integrated current of the reaction is constant (4.067 C). Calculation of the amount of Np(III) oxidized from the integrated current yields 1.40×10^{-2} mol L^{-1}. A neptunium concentration in the resulting stock solution of 1.39×10^{-2} mol L^{-1} is measured by liquid scintillation counting (LSC). The H^+ concentration (0.857 mol L^{-1}) is determined by titration with NaOH after removing the neptunium by cationic exchange. The neptunium oxidation state is checked by NIR absorption spectroscopy using a CARY 14 spectrometer on an aliquot of the stock solution diluted to 1/10 of its original concentration using 1 mol L^{-1} $HClO_4$. No evidence for Np(V) is observed; the freshly prepared Np(IV) solution contains only Np(IV). As the spectrum of the diluted Np(IV) stock solution does not change significantly after one week storage in air, we conclude the solution to be stable against oxidation to Np(V). By calculating the molar absorption coefficient for the Np(IV) ion using the measured absorbance and the Np(IV) stock solution concentration determined with LSC, a value of 202 L mol^{-1} cm^{-1} is obtained. This value is in good agreement with the value of 206 L mol^{-1} cm^{-1} reported in the literature [9].

A $-\log[H^+]$ 1.8 Np(IV) sample is prepared in a glove bag flushed with argon. The final neptunium concentration is 1.94×10^{-3} mol L^{-1} with a ionic strength of 0.123 mol L^{-1} $Na^+/HClO_4$ and $-\log[H^+] = 1.81 \pm 0.04$. The $-\log[H^+]$ is adjusted by adding small amounts (10–20 μl) of 1 mol L^{-1} NaOH. The $-\log[H^+]$ concentration is measured with a Ross combined glass electrode, which is calibrated for $-\log[H^+]$ values between 1 and 2 using known $HClO_4$ solutions before and after measuring the sample. The sample solution is transferred into a capped plastic cuvette. The cap is then sealed or glued tight with an epoxy resin. Comparison of the NIR spectra of this sample before and after irradiation with X-rays during the XANES/EXAFS measurements shows that Np(IV) in this sample is not stable in the synchrotron X-ray beam; in situ photo-oxidation of the Np(IV) to Np(V) is observed. We assume that the epoxy resin used to seal the cuvette containing the sample presumably acts as a catalyst for the photo-oxidation. A 3.1×10^{-3} mol L^{-1} Np(IV) solution in 1 mol L^{-1} $HClO_4$ containing the Np^{4+} aquo ion is observed to be more stable in the synchrotron X-ray beam and its XANES/EXAFS spectra are measured for comparison as a reference.

The Np(IV) oxyhydroxide precipitate is prepared by hydrolysis. Seventy micro litres of the $1.39 \cdot 10^{-2}$ mol L^{-1} Np(IV) stock solution is diluted with 1318 μL milliQ water and aliquots of 1 mol L^{-1} NaOH added until the precipitation of Np(IV) hydroxide is observed. This occurs at a $-\log[H^+]$ of 3.7. The suspension is then centrifuged over a Satorius ultrafiltration filter with a 20 000 Da cut-off. The filter with the precipitate is placed in a capped plastic cuvette and sealed in the same manner as the solution samples.

2.2. Preparation of Np(IV) and Np(V) solutions containing dissolved humic substances (HS)

The HS used for preparation of the Np(IV)–HS sample is a Boom clay fulvic acid (FA) solution. A FA solution is prepared by dissolving 57.8 mg FA in 1 mL 0.1 mol L^{-1} NaOH. The $-\log[H^+]$ is adjusted to approximately 2.2 by adding ~1 mL 0.1 mol L^{-1} $HClO_4$ and 1 mL milliQ water. One hundred and fifty micro litres of Np(IV) stock solution diluted to 2 mL with milliQ water is added to 1.05 mL of the FA solution. Following addition of 2.5 mL milliQ water the $-\log[H^+]$ is ~1.5. A neptunium concentration of 1×10^{-3} mol L^{-1} used is chosen to saturate this FA 5×10^{-4} eq. L^{-1} functional groups calculated from its proton exchange capacity (PEC). The PEC is the amount of titratable protons of the HS by acid–base titration and is 3 meq. g^{-1} for this particular Boom clay FA. After 20 h, the measured $-\log[H^+]$ value is 1.52 and the FA coagulated and settled to the bottom of the reaction vessel. The supernatant solution is removed carefully with a pipette and the residual suspension transferred into a 400 μL centrifuge tube and centrifuged for 20 min. The supernatant is removed from the top and 10 μL analyzed by LSC. The amount Np(IV) sorbed onto the FA is calculated by difference to be 87%. The samples are left in the centrifuge tubes and measured in the form of wet pastes. The tube opening stopper is glued with epoxy resin and the entire tube encased in a shrink-wrapped plastic covering.

The HS used for preparation of the Np(V)–HS sample is commercial available natural humic acid (HA) (Aldrich). A 9.45 mol L^{-1} aqueous HA solution is prepared in a N_2 flow box by dissolving 50 mg purified HA in 1 mL 0.109 mol L^{-1} carbonate-free NaOH. Following adjustment of the $-\log[H^+]$ to ~7 with 0.1 mol L^{-1} $HClO_4$, the total solution volume is brought up to 5 mL with 0.116 mol L^{-1} $NaClO_4$. Sixty micro litres of an aqueous solution of 3.6×10^{-2} mol L^{-1} Np(V) in 1 mol L^{-1} $HClO_4$ is added to 2 mL of this HA solution to yield

1.02×10^{-3} mol L^{-1} Np(V) in 8.91 g L^{-1} HA. The $-\log[H^+]$ value is initially 4.7 and then adjusted to 6.99 by adding 20 μL 1 mol L^{-1} NaOH then 60 μL 0.2 mol L^{-1} NaOH. An aliquot of the solution is placed in a 5 mm × 10 mm polyacrylic cuvette. The solutions are contained within the cuvette by a plastic plug insert, which is sealed with two layers of epoxy having absorbent between them, and covering with another plastic stopper. The cuvettes are mounted during measurement so that the 10 mm are directed towards the incident beam path.

2.3. XANES/EXAFS data acquisition and analysis

XANES/EXAFS measurements are performed at the advanced photon source (APS), at the BESSRC beamline 12BM, using a Si(1 1 1) double-crystal monochromator (DCM) with the storage ring operated in 'top-up' mode at 7 GeV with 100 mA. The 12BM beamline is equipped with a collimating and focusing mirror and the beam spot used is 0.5 mm^2. The incident beam is free of higher harmonic reflections, as is shown by the absence of the corresponding inelastic scattering peaks recorded with an energy dispersive detector. The spectra are calibrated against the first derivative XANES spectrum of a Zr foil, defined as 17.998 keV [10]. Spectra are recorded in both transmission and fluorescence mode. Argon filled ionization chambers and a 13-element energy dispersive ultra-pure Ge solid state detector for fluorescence detection are used. Samples are studied mounted in the Actinide Facility sample changer [11] for transport and measurement and kept in an argon atmosphere.

XANES spectra are isolated by first subtracting the background and normalizing the absorption to unity at 17.75 keV. The EXAFS data is extracted from the raw data using standard procedures (background subtraction, normalization, μ_0 spline function fit and subtraction, energy-to-k conversion, k^2-weighting) and the WinXAS program [12]. The ionization energy (E_0) used for conversion to wave vector ($k = 0.262(E - E_0)^{1/2}$) is defined as the energy of the white line maximum. The EXAFS data is fit to the EXAFS equation using the standard least squares fit procedure in the feffit program [13] in order to determine metric parameters describing the neptunium coordination to surrounding oxygen atoms (neighboring atomic distances (R), EXAFS Debye–Waller factors (σ^2), coordination numbers (N) and relative shift in E_0 (ΔE_0)). EXAFS are Fourier transformed (FT) in the k-range between 2.6 and 10.5 $Å^{-1}$ using symmetric square windows with Δk = 0.1 $Å^{-1}$ 'Hanning sills'. Fits are performed in R-space between the values for $R - \Delta$ of 0.9 and 2.65 Å. Single scattering backscattering amplitude and phase shift functions calculated using FEFF7 [14] and an amplitude reduction factor ($S_0{}^2$) of unity are used in the fits. A model of two oxygen shells is used for the three sample spectra analyzed. In one case, a single shell model is used for the fit and compared to the two shell model results. Both Np–O distances for the two shell model are allowed to vary in a fit to the Np(V)–HS sample Np L3 EXAFS. The value obtained for shortest oxygen distance in that fit (1.81 Å) is then held constant during fits to the other sample spectra.

3. Results and discussion

3.1. UV–vis spectroscopy

Fig. 1 shows the UV–vis absorption spectrum between 930 and 1040 nm for the Np(IV) sample prepared at $-\log[H^+]$ 1.8 after irradiation with X-rays for over 4 h during the XANES/EXAFS experiments. This sample spectrum is compared to the spectra of the Np^{4+} aquo species reference solution after over 4 h of irradiation with X-rays and to the 10-fold diluted Np(IV) stock solution after one week storage under ambient (air) conditions but no X-ray irradiation. The absorption intensity is normalized to 1×10^{-3} mol L^{-1} neptunium concentration. The spectra show two absorption bands at 960 and 980 nm, corresponding to Np(IV) and Np(V) ions. The Np(IV) sample prepared at $-\log[H^+]$ 1.8 contains Np(V) after irradiation. When comparing spectra of the diluted Np(IV) stock solution (1.39×10^{-3} mol L^{-1}) and the irradiated reference solution (3.1×10^{-3} mol L^{-1}), both with $-\log[H^+]$ near 0, we find that only the irradiated sample shows a Np(V) peak. This sample was irradiated while under an argon atmosphere, while the diluted Np(IV) stock solution was kept in air, but not irradiated with X-rays, and shows no significant Np(V) formation. We conclude that the oxidation of Np(IV) to Np(V) involves photo-oxidation by the X-ray beam.

3.2. XANES/EXAFS results

The inherent difficulty when determining oxidation states for neptunium from Np L3,2 edge XANES spectra is illustrated in Fig. 2. In this figure, Np L3 XANES spectra for aqueous Np(IV) and Np(V) solutions containing dissolved

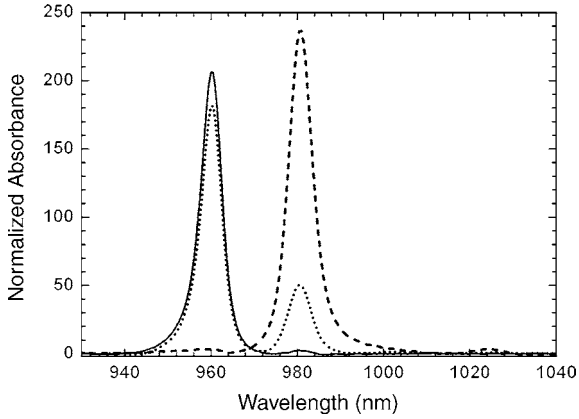

Fig. 1. Comparison of normalized UV–Vis absorption spectra of the diluted Np(IV) stock solution after one week under ambient (air) conditions (solid line), the Np^{4+} aquo ion reference solution with $-\log[H^+]$ 0 (dots), and the sample solution prepared at $-\log[H^+]$ 1.8 following 4 h irradiation with synchrotron X-rays under argon atmosphere (dashed line).

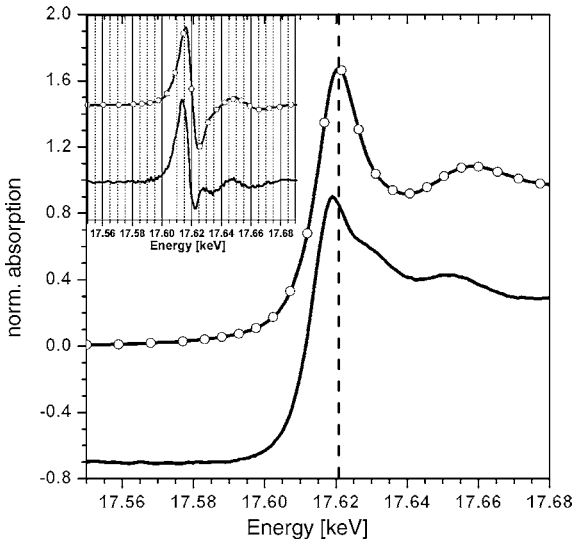

Fig. 2. Comparison of Np L3 edge XANES spectra for aqueous Np(IV) (top) and Np(V) (bottom) solutions containing dissolved HS. The inset shows the first derivative curves. The dashed line and grid lines are meant as a guide for the eye.

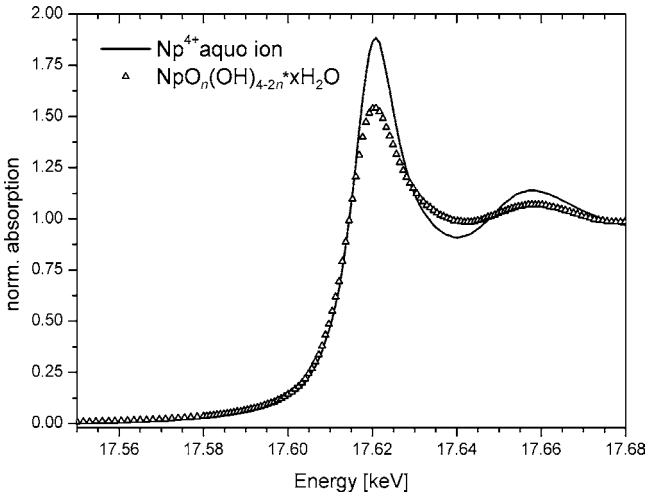

Fig. 3. Np L3 edge XANES for the Np^{4+} aquo ion (solid line) and a freshly precipitated Np(IV) oxyhydroxide (open triangles). Note the substantial decrease in white line intensity for the condensed system.

HS are compared. The inset depicts the corresponding first derivative curves. The energy positions of the white lines and inflection points, as maxima in the first derivative curves, are listed in Table 1. The energy position of the white line in the Np(V) XANES appears 1.8 eV below that for the Np(IV) sample spectrum; its inflection point is 2.4 eV lower. These shifts are comparable to those reported in [15]. The white line and inflection point energies are in reverse order of the expected increase in ionization energy with increasing valence state of the absorbing atom. This reverse order of absorption edge energy is associated with differences in XANES spectral resonances between Np(IV) and Np(V).

From comparing the spectra in Fig. 2, we might conclude that the white line intensity variation might be used to distinguish Np(IV) from Np(V). The intensity of the white line in the Np(IV) sample XANES is greater than that for the Np(V) sample in Fig. 2. However, the white line intensity generally varies not only with valence but also varies with the degree of condensation of the sample phase. This is illustrated in Fig. 3, where the first Np L3 XANES scan recorded for the Np^{4+} aquo ion reference solution is compared to that for freshly precipitated, solid Np(IV) oxyhydroxide. The white line height decreases substantially going from the solution to the solid, condensed system. This white line intensity decrease with increasing condensation is related to a decrease in the transition probability (P) of the $2p_{3/2}$ core electron to the dipole allowed 6d-like final state. In the solution species, the final state may be described using molecular orbitals (MO), whereas in the solid oxyhydroxide a band or electron cloud description is applicable. The density of states (DOS) in the MO description is higher than that in the band description. Because P increases with increasing DOS and vice versa, a lower DOS in the condensed system leads to a lowering of the white line intensity due to an associated decrease in P [16].

That these white line variations occur, independent of valence state, can be a source of error in individual concentration determinations of Np(IV) and Np(V) in mixtures. Linear combination of XANES spectra from reference compounds with a different degree of condensation than the unknown compound to be modeled will lead to erroneous results. For example, we simulated a spectrum of a hypothetical valence mixture having 50% Np(IV) and 50% Np(V) using the Np(IV) oxyhydroxide spectrum in Fig. 3 and the Np(V)–HA sample XANES in Fig. 2. Of course a least square fit to this simulated data using a linear combination of the XANES used to simulate the data itself (the Np(IV) oxyhydroxide and the Np(V):HA XANES), yields the expected ratio of Np(IV):Np(V) 50:50 with a $\Delta\chi^2$ of 0. However, if we use a different Np(IV) sample XANES in the linear combination such as the XANES for the Np^{4+} aquo species instead of the Np(IV) oxyhydroxide spectrum, we obtain an incorrect Np(IV):Np(V) ratio of 24:76 with the sum of $\Delta\chi^2$ = 0.12 (Fig. 4).

The most distinguishing differing feature between the Np(IV) and Np(V) spectra in Fig. 2 is the multiple scattering (MS) resonance at the high energy flank of the white

Table 1
Position of the inflection point and the white line of the XANES spectra shown in Figs. 2, 3 and 5

Sample/pH	Inflection point (eV)	White line (eV)
Np^{4+} aquo ion/0 (d)	17616.1	17620.9
Np(IV)/1.81 (b)	17615.2	17620.0
Np(IV) after 2.5 h irradiation/1.81 (a)	17615.3	17620.1
Np(IV)–HS/1.52	17616.0	17620.8
Np(V)–HS/6.99 (c)	17613.6	17619.0
Np(IV)/precipitated at ∼4	17615.7	17620.5

The letter designations given for four samples in parentheses correspond to the spectra depicted in Fig. 6.

line in the Np(V) sample spectrum characteristic for L3,2 edge XANES of 'yl' cations [17,18]. Its presence is clearly discernible in the first derivative curve between 17.625 and 17.630 keV. The MS feature results from scattering along the axial or 'yl' oxygen atoms (O_{ax}) of the linear neptunyl moiety [19] and appears approximately 10 eV above the white line, the exact position depending greatly on the actual Np–O_{ax} bond distance [20]. This MS feature is missing in the Np(IV) spectrum. The appearance of the MS feature can be used for distinguishing Np(V) as a neptunyl moiety from Np(IV). We will see below, however, that this MS feature is not easily discernible in XANES of valence state mixtures.

The subtle differences or lack of marked dissimilarity between the XANES of Np(IV) and Np(V) compounds renders it often advantageous to compare EXAFS spectra of Np(IV)/Np(V) valence mixtures. To illustrate this, Np L3 edge XANES and EXAFS spectra of the Np(IV) solution at $-\log[H^+]$ 1.8 recorded at the beginning of the X-ray experiments and following partial oxidation to Np(V) after 2.5 h in the X-ray beam (Fig. 1) are shown in Figs. 5 and 6. Data for the Np^{4+} aquo ion and for the Np(V)–HS sample are included in Fig. 6 for comparison. The formation of Np(V) in the solution sample during oxidation is not clearly evident in the XANES spectra. The shift in the energy position of the white line and inflection point in these spectra compared to the other Np(IV) samples is small. This shift is −0.8 or −0.9 eV when compared to the Np^{4+} aquo ion XANES (Table 1). This energy shift is about the same as the 0.8 eV step size between data points used in recording the spectra. The shift in the photo-oxidation samples XANES relative to the white line and inflection point in the precipitate is half as large, only −0.4 eV. The most prominent XANES feature distinguishing Np(IV) from Np(V), the MS feature associated with the neptunyl cation, is not obvious in the XANES

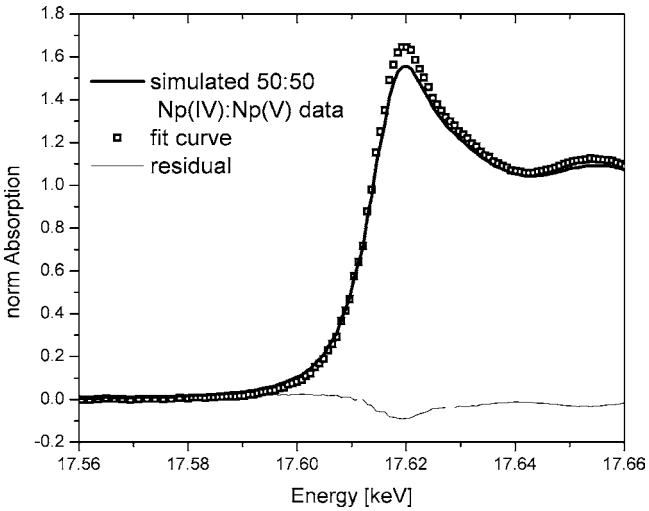

Fig. 4. Simulated Np L3 XANES for a 50:50 Np(IV):Np(V) mixture using the $NpO_n(OH)_{4-2n}{\cdot}xH_2O$ spectrum in Fig. 3 and the Np(V):HA XANES in Fig. 2 (thick solid line), the result from a least square fit using the Np(V):HA and Np^{4+} aquo ion spectra (squares), and the residual (thin line).

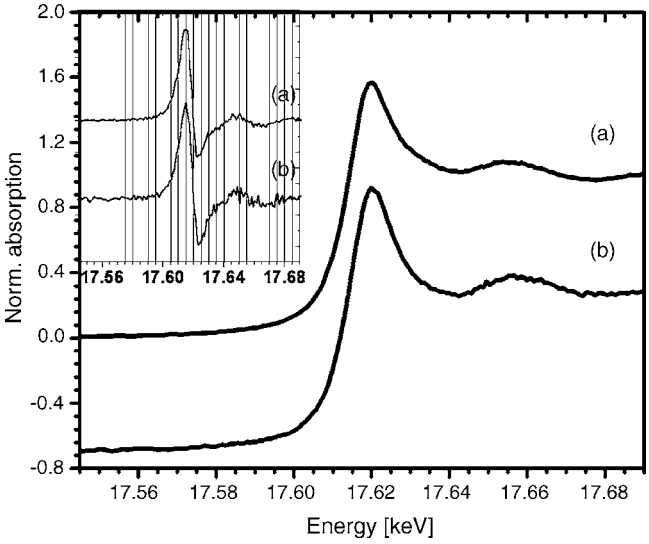

Fig. 5. Np L3 edge single scan XANES transmission spectra for a Np(IV) solution $-\log[H^+]$ 1.8 recorded during in situ photo-oxidation of approximately 20 min (b) and the same solution following 2.5 h in the X-ray beam (a). The first derivatives of the spectra are shown in the inset. Spectra are shifted along the *y*-axis for clarity.

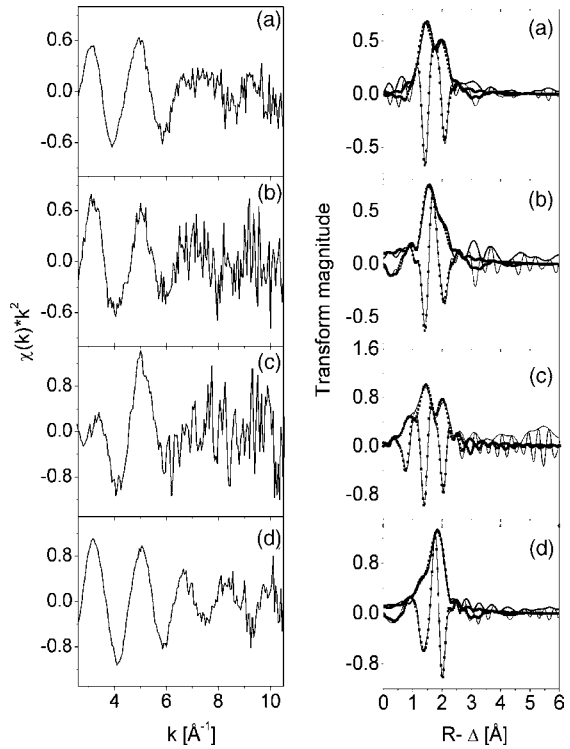

Fig. 6. Np L3 EXAFS (left) and their corresponding magnitudes and imaginary part of the Fourier transform for the oxidation samples, whose XANES are shown in Fig. 5 (a and b), the Np(V)–HS sample, whose XANES is in Fig. 2 (c), and the Np^{4+} aquo ion sample (d), whose XANES is depicted in Fig. 3. Note that the *y*-axis scale for the oxidation samples is smaller. Lines are experimental data and symbols fit results as described in the text.

of the solutions during oxidation. It is scarcely discernible in the first derivative curve of the first XANES recorded and not well-resolved in the spectrum after 2.5 h irradiation, appearing only as a shoulder. The white line intensity of the spectra for the solution prepared at $-\log[H^+]$ 1.8 is observed to decrease compared to that of the Np^{4+} aquo ion. Because, however, the white line intensity generally varies not only with valence but also varies with the degree of condensation of the sample phase (discussion above) this is not a direct indicator of the oxidation to Np(V). The observed white line intensity decrease could be erroneously interpreted here as being indicative of Np(IV) hydrolysis leading to colloid formation [7].

In contrast to the subtle XANES differences, the EXAFS of the solution prepared at $-\log[H^+]$ 1.8 is distinctly different than that of the Np^{4+} aquo ion (Fig. 6) for both irradiation times. Note that the Np^{4+} aquo ion spectrum shown is the initial scan of the sample. Because it was irradiated with beam for approximately 30 min while recording the scan, it presumably contains an insignificant amount of Np(V), as opposed to the amount of Np(V) formed in the sample following 4 h X-ray irradiation revealed by UV–vis spectroscopy (Fig. 1). The Np–O shell in the FT for the sample studied during oxidation exhibits two distances, as does the Np(V)–HS sample; the Np–O shell in the FT for the Np^{4+} aquo ion EXAFS shows only a single shell with a $R - \Delta$ maximum near 1.9 Å. The splitting of the Np–O shell is discernible in the EXAFS of the initial spectrum of the oxidation solution sample recorded at the begin of the photo-oxidation, and is well-resolved in the spectrum recorded 2.5 h later. The short Np–O distance visible near $R - \Delta$ = 1.55 Å (corresponding to an actual distance near 1.81 Å, Table 2) in the Np(V)–HS FT EXAFS corresponds to the interatomic distance in the neptunyl unit, $Np–O_{ax}$. The second Np–O shell in this FT corresponds to oxygen atoms bound to Np(V) in the neptunyl equatorial plane, $Np–O_{eq}$ [21]. The metrical parameters obtained from the least square fit to this data, modeled using two Np–O distances (Table 2), reflect the Np(V) pentagonal bipyramidal coordination with ∼2 O_{ax} at a 1.81 Å distance and ∼5 O_{eq} at 2.47 Å.

The Np^{4+} aquo ion EXAFS is fit using both a model of a single Np–O distance and a model of two Np–O distances, including the short 1.81 Å distance to represent the $Np–O_{ax}$ bond, which is held constant in the fits. The results for the two shell model yield positive amplitude for the $Np–O_{ax}$ shell EXAFS but with an extremely large value for σ^2. This large σ^2 makes the contribution of the EXAFS oscillation for this shell only significant at low k. Leaving this shell out of the fit and using a single Np–O shell model yields essentially the same results with a minor increase in the R-value (value of merit for the goodness of the fit) from 0.006 for the two shell fit to 0.007 for the single shell fit. Only the results for the single shell fit are listed in Table 2. It appears unlikely that the short Np–O distance (R(O1)) represents a true Np–O shell in this sample. Because Th(IV) also exhibits a similar short $R - \Delta$ FT feature [22,23] and is never present as a thorinyl cation, we suggest that the short $R - \Delta$ FT feature in this Np^{4+} aquo ion spectrum has a similar origin. This low frequency EXAFS contribution may be due to atomic contributions, to multi-electron excitations in the EXAFS-regime, or it could also simply be an artifact of the μ_0 spline function subtraction during isolation of the EXAFS from the raw data.

Table 2
Results from fits to the EXAFS data shown in Fig. 6

Spectrum	Shell	N	R (Å)	σ^2 (Å^2)	ΔE_0 (eV)
(a)	O1	0.7	1.81 (f)	0.000	−2.0
	O2	7.2	2.44	0.020	
(b)	O1	0.3	1.81 (f)	−0.006	−7.5
	O2	9.8	2.33	0.021	
(c)	O1	1.5	1.81	0.001	6.9
	O2	5.2	2.47	0.010	
(d)	O	8.7	2.39	0.007	−2.5

See text for details.

In contrast, fit results using two Np–O distances to the spectra of the oxidation samples suggest that the contribution of the $Np–O_{ax}$ shell to the EXAFS in these two samples is significant. The results for spectrum (a), the sample irradiated for 2.5 h, are similar to those for a neptunyl cation with a pentagonal bipyramidal coordination polyhedron. The value for N for $Np–O_{ax}$ is about half that observed for N(O1) in the Np(V)–HS sample. Because the amplitude parameters N and σ^2 are highly correlated, we try to fit the data holding the value for σ^2(O1) constant at 0.003 Å^2. The actinyl cations with their An-O_{ax} bond order of two or greater generally exhibit small σ^2 of 0.001–0.003 Å^2. In these fits, a small N(O1) of 1.1 is still obtained. The smaller than expected amplitude for the $Np–O_{ax}$ oscillation and the large σ^2 for the O_{eq} shell in this sample is likely an indication that Np(IV) is still in the sample.

The situation is more extreme for the results for the same solution but irradiated less, spectrum (b). Splitting of the Np–O shell from the presence of $Np–O_{ax}$ and $Np–O_{eq}$ is evident but evidence for Np(IV)–O distances is also present. The overlap of Np(IV)–O, $Np–O_{ax}$, and $Np–O_{eq}$ distances leads to a dampening of the overall or sum EXAFS amplitude. We obtain a negative σ^2 value for the $Np–O_{ax}$ shell in the fit and an unusually short R(O2) value. We also observe this fit to be very sensitive to changes in the model used. For example, if the value for σ^2(O1) is kept constant in addition to R(O1), then significantly different values for all of the parameters result. Obviously the model has not found any deep minimum; a model of only two shells is insufficient at describing the spectrum. The Np(IV)–O contribution must be significant and is not considered in the model. The neptunium in this sample has considerable amounts of both Np(IV) and Np(V) so that we expect different distances for the $Np–O_{ax}$, $Np–O_{eq}$, and Np(IV)–O bonds. Considering the data quality, the success of a three shell fit is questionable, however.

4. Conclusions

In conclusion we may summarize that evidence for the oxidation of Np(IV) in a solution sample through irradiation with synchrotron X-rays from their XANES spectra is not conclusive in our data. Changes in white line amplitude are a poor indicator, the energy shifts involved are slight, and the presence of the MS feature is uncertain, especially in the XANES spectrum with the least X-ray exposure (Fig. 5, spectrum (b)). Although these XANES indicators for the presence of Np(V) are not entirely convincing, analysis of this sample's EXAFS unequivocally reveals Np(V) formation.

Generally, the lack of marked dissimilarity between the XANES of Np(IV) and Np(V) compounds renders it important never to rely solely on XANES data for determining if Np(IV):Np(V) valence mixtures in neptunium samples occur; one must also check the EXAFS region. EXAFS analysis of L3 (L2) edge data will unlikely provide a precise quantitative method for determining Np(IV):Np(V) ratios in unknown samples. However, it can be used to make strong qualitative case, stronger than possible from XANES analysis alone for Np(V) formation should it occur.

Acknowledgements

M.P. Jensen is cordially acknowledged for his help in data acquisition. The BESSRC CAT at APS is gratefully acknowledged for beamtime allotment. Use of the infrastructures of the Actinide Facility for synchrotron research in the Chemistry Division of ANL is also acknowledged with gratitude. Use of the Advanced Photon Source was supported by the US Department of Energy, Office of Science, Office of Basic Energy Sciences, under Contract No. W-31-109-ENG-38.

References

[1] G. Bonsdorf, M.A. Denecke, K. Schafer, S. Christen, H. Langbein, W. Gunsser, Solid State Ionics 351 (1997) 101–103;
P.-E. Petit, F. Farges, M. Wilke, V.A. Solé, J. Synchrotron Rad. 8 (2001) 952.
[2] M.A. Denecke, K. Janssens, K. Proost, J. Rothe, HASYLAB Annual Report 2003. http://www-hasylab.desy.de/science/annual_reports/2003_report/index.html.
[3] M.R. Antonio, L. Soderholm, J. Alloys Compd. 250 (1997) 541.
[4] C.S. Wright, R.I. Walton, D. Thompsett, J. Fisher, Inorg. Chem. 43 (2004) 2189.
[5] S.D. Conradson, I. Al Mahamid, D.L. Clark, N.J. Hess, E.A. Hudson, M.P. Neu, P.D. Palmer, W.H. Runde, C.D. Tait, Polyhedron 17 (1998) 599.
[6] F. Farges, C.W. Ponader, G. Calas, G.E. Brown Jr., Geochim. Cosmochim. Acta 56 (1992) 4205.
[7] J. Rothe, M.A. Denecke, V. Neck, R. Mueller, J.I. Kim, Inorg. Chem. 41 (2002) 249.
[8] C. Walther, J. Rothe, M.A. Denecke, T. Fanghänel, Inorg. Chem 43 (2004) 4708–4718.
[9] V. Neck, J.I. Kim, B.S. Seidel, C.M. Marquardt, K. Dardenne, M.P. Jensen, W. Hauser, Radiochim. Acta (2001) 89.
[10] W.H. McMaster, N. Kerr Del Grande, J.H. Mallett, J.H. Hubbell, Lawrence Livermore National Laboratory Report, UCRL-50174, Section II, Revision I, 1969.
[11] http://chemistry.anl.gov:80/heavy-element/actinide/multiple.html
[12] T. Ressler, J. Phys. IV 7 (1997) C2–C269.
[13] E.A. Stern, M. Newville, B. Ravel, Y. Yacoby, D. Haskel, Physica B 208/209 (1995) 117.
[14] J.J. Rehr, R.C. Albers, S.I. Zabinsky, Phys. Rev. Lett. 69 (1992) 3397.
[15] L. Soderholm, M.R. Antonio, C. Williams, S.R. Wasserman, Anal. Chem. 71 (1999) 4622.
[16] D. Bazin, D. Sayers, J.J. Rehr, C. Mottet, J. Phys. Chem. B 101 (1997) 5332.
[17] D. Petit-Maire, Thesis dissertation, University of Paris 6, 1998 (in French).
[18] C. Den Auwer, E. Simoni, S. Conradson, C. Madic, Eur. J. Inorg. Chem. (2003) 3843.
[19] E.A. Hudson, P.G. Allen, L.J. Terminello, M.A. Denecke, T. Reich, Phys. Rev. B 54 (1996) 156–165.
[20] M.A. Denecke, Proceedings of the OECD-NEA Workshop on Speciation Techniques and Facilities for Radioactive Materials at Synchrotron Light Sources, Grenoble, France, 4–6 October, 1998, pp. 135–141.
[21] M.R. Antonio, L. Soderholm, C.W. Williams, Radiochim. Acta 89 (2001) 17.
[22] M.A. Denecke, D. Bublitz, J.I. Kim, H. Moll, I. Farkes, J. Synchrotron Rad. 6 (1999) 394.
[23] V. Neck, R. Müller, M. Bouby, M. Altmaier, J. Rothe, M.A. Denecke, J.I. Kim, Radiochim. Acta 90 (2002) 485.